




Research Article

Multiband superconductivity in $\text{SrFe}_{2-x}\text{Ni}_x\text{As}_2$

A. S. Usoltsev¹ · A. V. Sadakov¹ · O. A. Sobolevskiy¹ · V. A. Vlasenko¹ · K. S. Pervakov¹ · E. A. Polianskaya¹ · E. I. Maltsev¹ 

Received: 28 December 2021 / Accepted: 25 April 2022

Published online: 13 May 2022

© The Author(s) 2022 [OPEN](#)

Abstract

In this paper, we present a detailed study of the upper critical field and the energy gap structure of $\text{SrFe}_{2-x}\text{Ni}_x\text{As}_2$ single crystals with different nickel doping levels. Superconducting transitions were measured resistively in longitudinal and transverse magnetic fields up to 16T. The anisotropy of the upper critical field $H_{c2}||ab/H_{c2}||c$ decreases monotonically to 1.4 with decreasing temperature for all measured samples. The WHH model was not able to fit measured $H_{c2}(T)$ temperature dependences well, but the effective two-band model is in good agreement with the data and anisotropy behavior. Values and temperature dependences of superconducting gaps were determined directly by multiple Andreev reflection spectroscopy on symmetrical SnS junctions. Andreev reflections study revealed two superconducting gaps; our data are in line with the experimental results on most iron-based superconductors.

Article highlights

We obtained values and temperature dependencies of two distinct energy gaps in $\text{SrFe}_{2-x}\text{Ni}_x\text{As}_2$ (Sr-122) superconductor. This is important addition to multiband super-

conductivity studies in Sr-122 system. Upper critical field temperature dependencies in $H||c$ and $H||ab$ orientations are analyzed in terms of two band model.

Keywords Superconducting energy gaps · Upper critical field · Iron-based superconductors

1 Introduction

The discovery of iron-based superconductors (IBSC) [1] is undoubtedly a substantial milestone in solid state physics. The family of IBSC is vast and versatile, and to this day it brings many challenges to the scientific community both theoretical and experimental ones. A parent compound of a typical IBSC (though there are several exceptions [2]) is a stripe antiferromagnetic semimetal, which does not show superconducting transition. However, the

superconducting phase starts to emerge when magnetic order is suppressed by electron or hole doping, external or chemical pressure. The superconducting phase starts to emerge with critical temperatures up to 53–57 K [3–5] in 1111 family (with formula REFeAsO , RE—rare earth element), up to 38 K [6] in 122 family (MFe_2As_2 , M—Ba, K, Sr etc.), up to 9–37 K ([7, 8]) in 11 family (FeSe , FeS systems). In the typical 122-type iron-based superconductors, parent compounds (BaFe_2As_2 , SrFe_2As_2 , CaFe_2As_2) and under-doped samples undergo a structural transition

Supplementary information The online version contains supplementary material available at <https://doi.org/10.1007/s42452-022-05047-3>.

✉ E. I. Maltsev, malcevei@lebedev.ru | ¹P.N. Lebedev Physical Institute, Russian Academy of Sciences, Moscow, Russia 119991.



SN Applied Sciences

(2022) 4:171

| <https://doi.org/10.1007/s42452-022-05047-3>

from tetragonal to orthorhombic phases, usually accompanied with nematic ordering at the temperature T_c , followed by an AFM ordering transition. Depending on the doping (or pressure) level one can study different kinds of superconducting phases within the same system [9]. The common feature for all different IBSC systems and phases is the complex multiband nature of superconductivity.

The Ni-doped SrFe_2As_2 system belongs to the 122 family. The parent compound undergoes a lattice distortion and AFM ordering at $T_0=205\text{ K}$ [10], and Ni substitution of the Fe positions in the parent compound leads to a fast decrease of T_0 until the transition is fully suppressed at $x=0.16$. Along with the T_0 suppression, bulk superconductivity appears at $x=0.1$. In $\text{SrFe}_{2-x}\text{Ni}_x\text{As}_2$ compound the superconductivity exists in concentration range $0.10 \leq x \leq 0.22$ (maximum T_c of about 9 K). Such low T_c among the 122 system compounds is observed only in $\text{SrFe}_{2-x}\text{Ni}_x\text{As}_2$ and $\text{SrFe}_{2-x}\text{Pd}_x\text{As}_2$ [11] compounds. Taking into account very flat SC 'dome' on the phase diagram approximately, flat region starts with $x=0.12$ and ends with $x=0.17$, one can argue that this system is a rather unusual member of the 122 IBSC. And our goal is to study its fundamental superconducting parameters—energy gap and upper critical field [$H_{c2}(T)$] and their peculiarities arise from the multiband nature of the compound and their evolution with changes in doping level. We carried out resistive transport experiments $R(T, H)$ in magnetic fields up to 16 T to investigate upper critical field temperature dependence. For energy gap studies Andreev reflection spectroscopy of the symmetrical Superconductor-normal metal-Superconductor (S-n-S) junctions was used, this technique is a unique probe of the superconducting order parameters [12, 13].

The paper is organized in the following structure. In Sect. 1 we provide brief overview of the current state of the iron-based superconductors field. Section 2 provides details on crystal growth and samples characterization. In Sect. 3 we present study of the upper critical field behavior, and compare it to two-band theoretical model. Section 4 shows the Andreev reflection spectroscopy investigations of the superconducting order parameter. In Sect. 5 we summarize the results of the article.

2 Crystal growth and experimental details

All preparations for synthesis were conducted in a glove box with an Ar atmosphere ($\text{O}_2 < 1\text{ ppm}$, $\text{H}_2\text{O} < 1\text{ ppm}$). $\text{SrFe}_{2-x}\text{Ni}_x\text{As}_2$ single-crystals of different compositions ($x=0.13, 0.17$ by initial components ratio) were grown by the self-flux method with $\text{Fe}_{2-x}\text{Ni}_x\text{As}_2$ mixture as a flux. We prepared precursors $\text{Fe}_{2-x}\text{Ni}_x\text{As}_2$ of corresponding compositions; metallic arsenic in pieces (99.9999%), iron grains (99.98%), and nickel

in form of swarf (99.9%) were sealed in the quartz tube with a residual Ar pressure of 0.2 atm. The quartz tube was heated up in a muffle furnace up to 600 °C and held at this temperature for 72 h to bond As with Fe and Ni elements, slowly heated to 900 °C and held for 72 h, heated to 1000 °C and held for 48 h.

Mixtures of high-purity (99.8%) metallic Sr and $\text{Fe}_{2-x}\text{Ni}_x\text{As}_2$ precursor with the ratio of 1:3 were loaded in alumina crucibles that were afterwards sealed in Nb containers under Ar pressure of about 0.3 atm. Containers were heated to 1200 °C at the rate of 100 °C/h in a tube furnace, kept at the temperature for 12 h, and cooled down to 900 °C at the rate of 1.5 °C/h. After that, the furnace was turned off and containers slowly cooled down to room temperature. Synthesized crystals were separated from flux by mechanical treatment; they had the form of shiny plates with lateral sizes of 1–4 mm and thickness about 0.1–0.2 mm.

The actual composition of single crystals was investigated by energy-dispersive X-ray spectroscopy (EDX) with the scanning electron microscope (SEM) JEOL JSM 7001FA and refined by X-ray diffractometry (XRD) with Rigaku MiniFlex 600 diffractometer (see Suppl. Mat.). By the averaging results of several EDX measurements on the surface, it was found that Ni concentration in the resulting crystals is about 10% lower than the nominal concentration value. That fact is consistent with the previous experience of synthesizing Ni-doped iron-based compounds [14, 15]. In present work, crystals were labeled by their actual composition: $x=0.12$ and $x=0.15$.

Crystals are insensitive to the air atmosphere for periods of about a few weeks, however we found insignificant signs of crystals degradation that remained in the air for a year.

For magnetotransport measurements, current and potential indium contacts with a resistance less than 1 Ω were prepared on the surface of each sample. Measurements were carried out in a CFMS-16T cryomagnetic system in constant magnetic fields up to 16 T with a help of a Keithley 6221 power supply and a Keithley 2182 nanovoltmeter. We studied the temperature and magnetic field dependences of the longitudinal resistance in $H||c$ and $H||ab$ orientations. All magnetic measurements were made with a Quantum Design PPMS-9. Figure 1 presents AC-susceptibility temperature dependences of $\text{SrFe}_{2-x}\text{Ni}_x\text{As}_2$ single crystals ($x=0.12$ and $x=0.15$). The nearly optimally doped ($x=0.15$), and underdoped samples ($x=0.12$) have almost the same critical temperature due to the flat dome shaped superconducting phase diagram. Inset shows microphotography of one of single crystals obtained with the SEM.

Andreev reflections (AR) spectra were measured using two SR-830 lock-in amplifiers for independent measurements dI and dV , National Instruments acquisition card, and custom made state-of-the-art preamplifier board with voltage controlled current source.

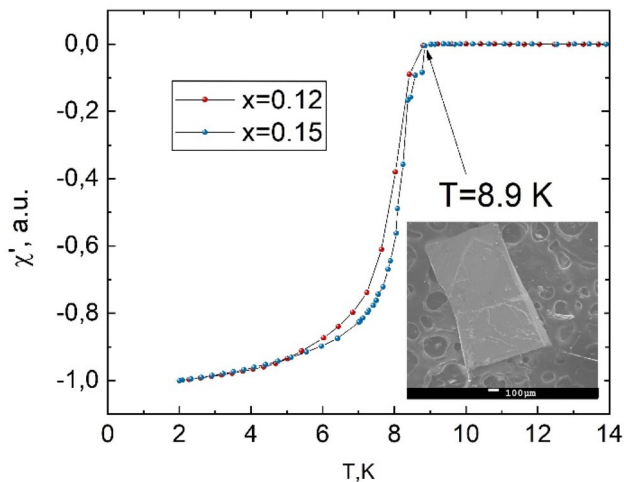


Fig. 1 AC susceptibility temperature dependences of SrFe_{2-x}Ni_xAs₂ single crystals with H_{ac}=5 Oe. Inset: The photo of the as-grown SrFe_{1.85}Ni_{0.15}As₂ single crystal

3 Upper critical field temperature behavior

The results of the magnetotransport measurements of the SrFe_{2-x}Ni_xAs₂ single crystal (with x=0.12 and 0.15) in magnetic fields up to 16 T are shown in Fig. 2a to d. Our experimental data is consistent with previous works [14, 16] For

the upper critical field determination from R(T,H) curves, we used several criteria, i.e.: intersection of R(T) steep linear extrapolation and R=0 line (R=0 criterium), 50% of normal state resistivity criterium (R=50%), and 90%. The H_{c2}(T) curves with R=0 criteria are shown in Fig. 3 and 50% and 90% cases one can find in supplementary materials.

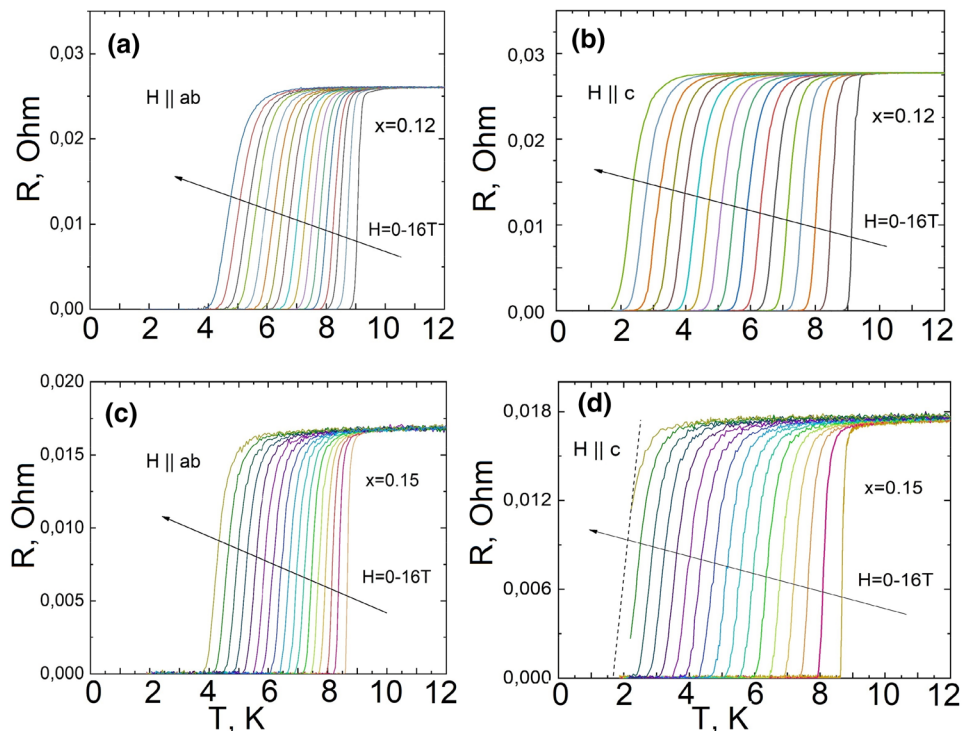
In order to describe H_{c2}(T) dependence of SrFe_{2-x}Ni_xAs₂ we first used the single band isotropic WHH model in dirty limit [17] which takes the form:

$$\ln\left(\frac{1}{t}\right) + \psi\left(\frac{1}{2}\right) = \left(1 + \frac{i\lambda_{so}}{4\gamma}\right)\psi\left(\frac{1}{2} + \frac{h + \lambda_{so}/2 + i\gamma}{2t}\right) + c.c.,$$

where c.c. stands for the complex conjugate term; t is dimensionless temperature T/T_c , $h = -4H_{c2}/(\pi^2 dH_{c2}/dt)$; ψ is the digamma function; λ_{so} and α are spin-orbit interaction parameter and Maki parameter, respectively; $\gamma = \sqrt{(\alpha h)^2 - \lambda_{so}^2}/4$. Spin-orbit scattering and Maki parameter represent the spin-orbital and spin-paramagnetic effects of magnetic field on Cooper pairs. This model was developed for superconductors with weak electron-phonon coupling and one isotropic band.

WHH model is not in a good agreement with experimental data for H||c case, but for H||ab it describes the data rather well (Fig. 3). Thus, single band isotropic model

Fig. 2 R(T, H) data measured in various magnetic fields with the H||ab and H||c orientations up to 16 T for the SrFe_{2-x}Ni_xAs₂ (x=0.12, 0.15)



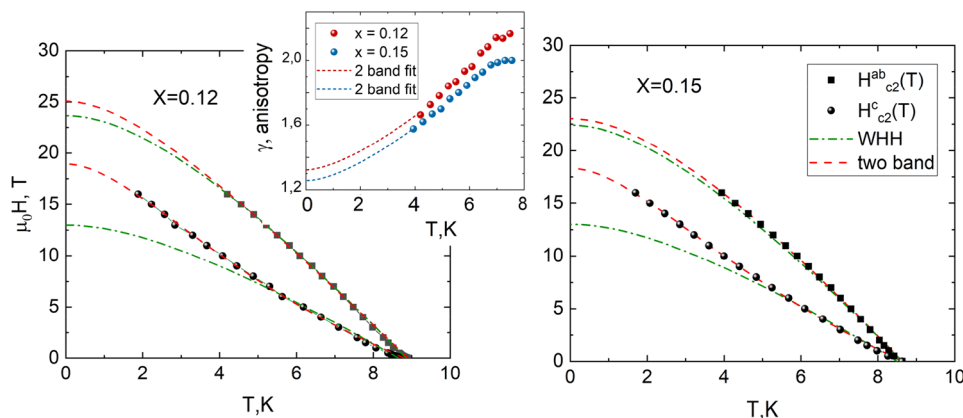


Fig. 3 Temperature dependence of the upper critical field obtained from $R(T, H)$ data with the in-plane and out-of-plane orientations. Left panel show data for $x=0.12$, right panel shows data for $x=0.15$. Dash-dotted lines show the WHH model approximation. Dash lines

show approximation of experimental data by the two-band model. Inset: The anisotropy of the upper critical field $\gamma = H_{c2}^c || ab / H_{c2}^c || c$; the $\gamma(0)$ was calculated from the two-band model approximation

cannot be used to describe behavior of the upper critical field in $SrFe_{2-x}Ni_xAs_2$ superconductor.

Gurevich two-band model takes into account the multi-band structure of superconductors. In this work, we apply Gurevich two-band model in dirty limit with spin-orbital effects [15]:

$$\ln(t) = - \frac{[U(h) + U(\eta h) + (\lambda_0/w)]}{2} + \left[\frac{(U(h) - U(\eta h) - (\lambda_-/w))^2}{4} + \frac{\lambda_{12}\lambda_{21}}{w^2} \right]^{1/2},$$

where $U(x) = \psi(1/2 + x) - \psi(1/2)$, $h = H_{c2}D_1\hbar/2\varphi_0k_B T$, $t = T/T_c$, φ_0 is the flux quantum, λ is the coupling constants matrix (diagonal and off-diagonal elements quantify the intraband and interband coupling, respectively), $\eta = D_2/D_1$, D_n is diffusivity of the n th band, λ_0 , λ_- and w are determined from λ . To reduce the number of the free parameters, we used the condition $\lambda_{12} = \lambda_{21}$ as only their product appears in the model.

Data was fitted well for both field orientations within the two-band model; fitting results are shown in Fig. 3, and fit parameters and coherence lengths for $R=0$ criteria are listed in Table 1, other fitting parameters one can find in supplementary materials. Coherence lengths were calculated from extrapolated values of $H_{c2}(0)$ using formulas $\xi^{ab} = \sqrt{\varphi_0/2\pi H_{c2}^c}$ and $\xi^c = \varphi_0/2\pi \xi^{ab} H_{c2}^{ab}$. In the case of $x=0.12$, diffusivities obtained from the fit can be interpreted as one band with strong anisotropy (band 1, $D^c/D^{ab} \approx 12$) and almost isotropic band (band 2, $D^c/D^{ab} \approx 1$) as was shown in our previous work on this system [16]. For $x = 0.15$, the results are similar with the only difference in ratios of diffusivities ($D^c/D^{ab} \approx 6.6$ and 0.5 for bands 1 and 2, respectively). Comparing products of diagonal and off-diagonal

elements of λ , we determined that both samples show significant interband coupling. The obtained diffusivity values are similar to those found in other iron-based superconductor with strontium

$Sr_{1-x}Eu_x(Fe_{0.89}Co_{0.11})_2As_2$ [18], but lower than in $BaFe_{2-x}Ni_xAs_2$ superconductor [19]. It should be mentioned

that 50% and 90% criteria are qualitatively in agreement with $R=0$, however the higher criterium percentage we take the fewer experimental points in $H-T$ diagram we have. In general, this leads to higher uncertainty of fitting parameters.

According to theory, two-band model is simplified to De Gennes–Maki equation for one-gap superconductor if $D_1/D_2 = 1$ [17, 20–22]. In our case for $H || ab$ orientation we have D_1/D_2 close to 1, therefore WHH model is in a good agreement with experiment.

According to Gurevich work, band with lower diffusivity dominates at temperatures close to 0 and band with higher diffusivity dominates at temperatures close to T_c [23]. Thus, for both samples, anisotropic band define behavior of $SrFe_{2-x}Ni_xAs_2$ close to T_c and with lowering temperature more isotropic band starts to manifest itself. It can be clearly seen on the anisotropy vs. T plot (inset Fig. 3): with decreasing temperature anisotropy decreases as well. Similar anisotropy behavior was also observed in $Sr_{1-x}Eu_x(Fe_{0.89}Co_{0.11})_2As_2$ [18].

4 Andreev reflections spectroscopy

We use Andreev reflection spectroscopy of symmetrical S-n-S junctions to measure the order parameter values [12]. The main advantage of this technique is that the gap values are directly extracted from the dI/dV spectra and no additional fitting procedures are needed. The SnS contacts were obtained by means of “break junction” technique—the sample is cleaved at a very low temperature (~ 2.0 K) forming a structure with bulk superconducting banks splitted up by a constriction in-between [24–26]. Since IBSC behave as rather good metals in the normal state, constriction acts as a normal metal. I–V curves of such contacts exhibit a so-called subharmonic gap structure (SGS)—a series of features corresponding to bias voltages $V_n = 2\Delta/en$, where $n = 1, 2, 3 \dots$ is a natural number equals to the number of Andreev reflection. Here, Δ is an energy gap value, e is the electron charge, n is the number of Andreev reflections. If several order parameters exist in the sample, then each gap will form independent SGS. Additionally, during the experiment it is possible to obtain a stack of SnS junctions, connected in series, in this case the bias voltage of SGS features will be multiplied by the number of contacts in the stack m : $V_{n,m} = (2\Delta/en) \times m$.

During the experiment, the sample is attached to the plane bronze spring through auxiliary flex printed circuit board (for signals measuring and isolation). Screw on the opposite side of the spring can bend the spring to vary the

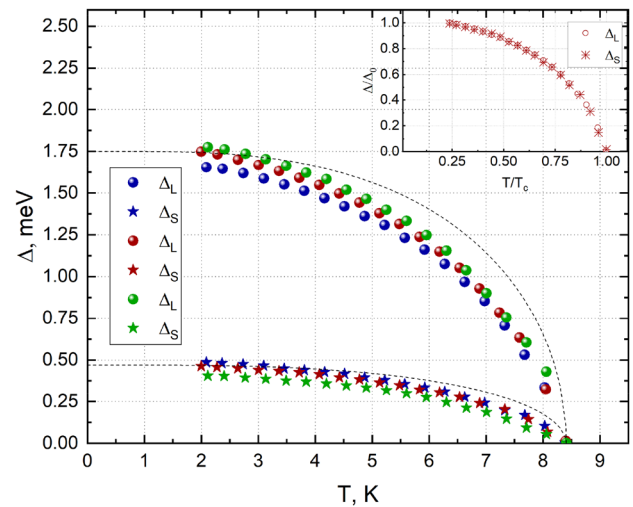


Fig. 5 Temperature dependences of gap values. Inset shows scaled temperature dependencies for both large and small gaps. Dashed lines represent a BCS-like fit

distance between superconducting banks. Thus one can rearrange the junction and obtain different contacts to collect statistics. In the experiments with layered superconductors, like IBSC samples, delaminate in the c direction thus the current in the junction flows parallel to the c axis.

Figure 4 depicts a normalized differential conductance for 3 different contacts obtained at $T \sim 2.0$ K on the

Fig. 4 **a** Normalised dI/dV characteristic for 3 different contacts. Grey vertical bars show biases for doubled values of large and small gaps. **b–d** Temperature evolution of characteristics from **(a)**, colors preserved. Characteristics cross y-axis roughly at the temperature it was measured

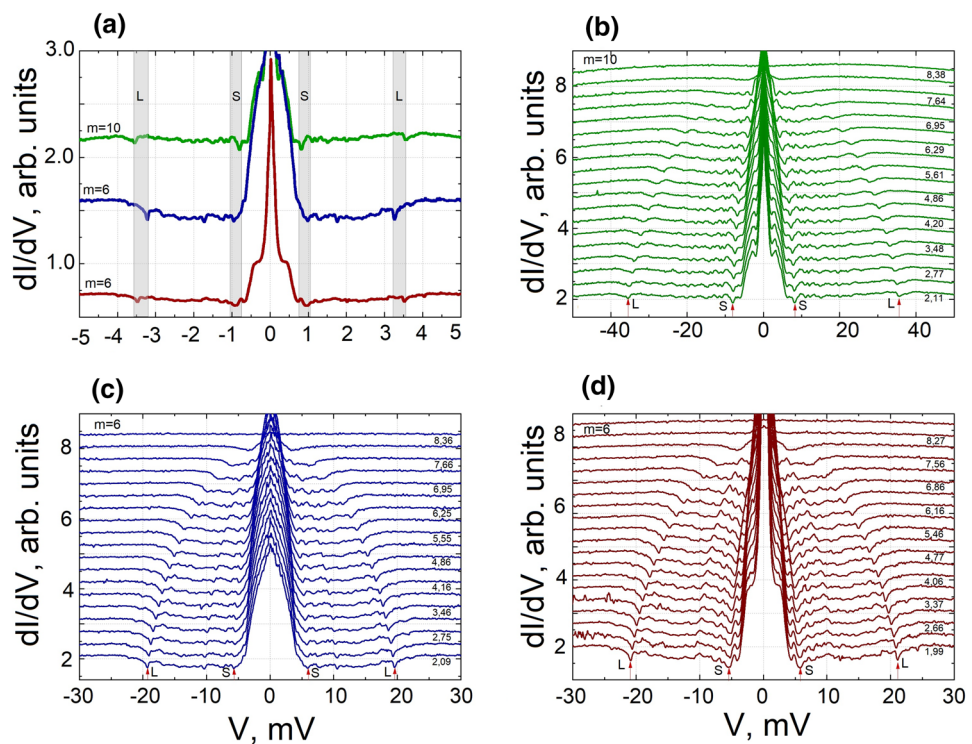


Table 1 Summary of the parameters for the upper critical field ($R=0$ criterium) and energy gaps

		$H_{c2}(0)$ (T)	ξ_{GL} (nm)	D_1 (cm ² /s)	D_2 (cm ² /s)	Δ_L (meV)	Δ_S (meV)
x=0.12	H c	19	4.2	2.06	0.20	–	–
	H ab	25	3.1	0.17	0.21		
x=0.15	H c	18	4.2	1.92	0.21	1.75	0.47
	H ab	23	3.4	0.29	0.39		

SrFe_{1.85}Ni_{0.15}As₂ sample. For all 3 spectra there are distinct features at biases around 3.55mV and 0.9mV. In Fig. 4b to d one can find temperature evolution of those spectra for red, blue and black curves from Fig. 4a correspondingly. For visual clarity spectra were shifted vertically so their sides cross vertical axis at values that roughly correspond to the temperature they were measured at. One can see that when the temperature rises the deeps smear and move toward lower biases until spectra become Ohmic at local T_c . Both deeps disappear at the same temperature and can't be derived from each other by normalization on any natural number so those features correspond to different order parameters. Figure 5 shows gaps values extracted from the temperature dependencies in Fig. 4b to d and a BCS-like fit (dashed lines) for visual reference. One can see a smooth decrease of gaps values with a temperature rising. Extrapolation to $T=0$ K gives us gaps values: $\Delta_L = 1.75$ meV, $\Delta_S = 0.47$ meV with corresponding characteristic BCS ratios: $2\Delta_L/k_bT_c = 4.83$, $2\Delta_S/k_bT_c = 1.27$. The obtained ratios for the investigated samples are typical for the IBSC 122-family, which implies the same pairing mechanism as in other 122 systems and in related 1144 system [13, 26].

5 Conclusions

We confirm the existence of multigap superconductivity in the Ni-doped SrFe₂As₂ system by various experimental methods. The values and temperature dependencies of the superconducting order parameters were obtained by means of Andreev reflection spectroscopy. The obtained BCS ratios for the investigated samples are typical for the 122 IBSC family. The analysis of the $H_{c2}(T)$ curves shows that the two-band model fits the experiment very well, thus confirming the multiband nature of the superconductivity in this system. The results of the two-band approximation suggest that the anisotropic band contribution dominates near T_c , whereas the main contribution at low temperatures comes from the isotropic band with a lower diffusion coefficient.

Acknowledgements In our measurements, we used equipment at the Shared Research Facilities Center in Lebedev Institute of Physics of

the Russian Academy of Sciences. This work was partially supported by the Russian Scientific Foundation (grant number 21-72-20114). K.S.P. acknowledges support by the Russian Scientific Foundation (RSF Project No. 21-12-00394).

Funding This work was supported by the Russian Scientific Foundation grant number 21-72-20114. K.S.P. has received research support from the Russian Scientific Foundation (Grant number 21-12-00394).

Declarations

Conflict of interest The authors of this paper declare that they have no conflict of interest.

Open Access This article is licensed under a Creative Commons Attribution 4.0 International License, which permits use, sharing, adaptation, distribution and reproduction in any medium or format, as long as you give appropriate credit to the original author(s) and the source, provide a link to the Creative Commons licence, and indicate if changes were made. The images or other third party material in this article are included in the article's Creative Commons licence, unless indicated otherwise in a credit line to the material. If material is not included in the article's Creative Commons licence and your intended use is not permitted by statutory regulation or exceeds the permitted use, you will need to obtain permission directly from the copyright holder. To view a copy of this licence, visit <http://creativecommons.org/licenses/by/4.0/>.

References

1. Kamihara Y, Watanabe T, Hirano M, Hosono H (2008) Iron-based layered superconductor La[O_{1-x}F_x]FeAs ($x = 0.05 - 0.12$) with $T_c = 26$ K. *J Am Chem Soc* 130:3296. <https://doi.org/10.1021/ja800073m>
2. Sato T, Nakayama K, Sekiba Y, Richard P, Xu Y-M, Souma S, Takahashi T, Chen GF, Luo JL, Wang NL, Ding H (2009) Band structure and fermi surface of an extremely overdoped iron-based superconductor KFe₂As₂. *Phys Rev Lett* 103:047002. <https://doi.org/10.1103/PhysRevLett.103.047002>
3. Khlybov EP, Omelyanovsky OE, Zaleski A, Sadakov AV, Gizatulin DR, Kulikova LF, Kostuleva IE, Pudalov VM (2009) Magnetic and superconducting properties of FeAs-based high-T_c superconductors with Gd. *JETP Lett* 90:387–390. <https://doi.org/10.1134/S0021364009220123>.
4. Chen XH, Wu T, Wu G et al (2008) Superconductivity at 43 K in SmFeAsO_{1-x}F_x. *Nature* 453:761–762. <https://doi.org/10.1038/nature07045>
5. Wei Z, Li H, Hong W et al (2008) Superconductivity at 57.3 K in La-doped iron-based layered compound Sm_{0.95}La_{0.05}O_{0.85}F_{0.15}FeAs. *J Supercond Nov Magn* 21:213–215. <https://doi.org/10.1007/s10948-008-0327-y>

6. Rotter M, Tegel M, Johrendt D (2008) Superconductivity at 38 K in the iron arsenide $(\text{Ba}_{1-x}\text{K}_x)\text{Fe}_2\text{As}_2$. *Phys Rev Lett* 101:107006. <https://doi.org/10.1103/PhysRevLett.101.107006>
7. Vedenev SI, Piot BA, Maude DK, Sadakov AV (2013) Temperature dependence of the upper critical field of FeSe single crystals. *Phys Rev B* 87:134512. <https://doi.org/10.1103/PhysRevB.87.134512>
8. Medvedev S, Mc Queen T, Troyan I et al (2009) Electronic and magnetic phase diagram of $\beta\text{-Fe}_{1.01}\text{Se}$ with superconductivity at 36.7 K under pressure. *Nat Mater* 8:630–633. <https://doi.org/10.1038/nmat2491>
9. Zou Q, Fu M, Wu Z et al (2021) Competitive and cooperative electronic states in $\text{Ba}(\text{Fe}_{1-x}\text{T}_x)_2\text{As}_2$ with T = Co, Ni, Cr. *npj Quantum Mater* 6:89. <https://doi.org/10.1038/s41535-021-00385-8>
10. Krellner C, Caroca-Canales N, Jesche A, Rosner H, Ormeci A, Geibel C (2008) Magnetic and structural transitions in layered iron arsenide systems: AFe_2As_2 versus RFeAsO . *Phys Rev B*. <https://doi.org/10.1103/PhysRevB.78.100504>
11. Han F, Zhu X, Cheng P, Mu G, Jia Y, Fang L, Wang Y, Luo H, Zeng B, Shen B, Shan L, Ren C, Wen H-H (2009) Superconductivity and phase diagrams of the 4d- and 5d-metal-doped iron arsenides $\text{SrFe}_{2-x}\text{M}_x\text{As}_2$ (M = Rh, Ir, Pd). *Phys Rev B* 80:024506. <https://doi.org/10.1103/PhysRevB.80.024506>
12. Kümmel R, Günsenheimer U, Nicolisky R (1990) Andreev scattering of quasiparticle wave packets and current–voltage characteristics of superconducting metallic weak links. *Phys Rev B* 42:3992. <https://doi.org/10.1103/PhysRevB.42.3992>
13. Kim TK, Pervakov KS et al (2021) Electronic structure and coexistence of superconductivity with magnetism in $\text{RbEuFe}_4\text{As}_4$. *Phys Rev B* 103:174517. <https://doi.org/10.1103/PhysRevB.103.174517>
14. Saha SR, Butch NP, Kirshenbaum K, Paglione J (2009) Evolution of bulk superconductivity in SrFe_2As_2 with Ni substitution. *Phys Rev B* 79:224519. <https://doi.org/10.1103/PhysRevB.79.224519>
15. Butch NP, Saha SR, Zhang XH, Kirshenbaum K, Greene RL, Paglione J (2010) Effective carrier type and field dependence of the reduced- T_c superconducting state in $\text{SrFe}_{2-x}\text{Ni}_x\text{As}_2$. *Phys Rev B* 81:024518. <https://doi.org/10.1103/PhysRevB.81.024518>
16. Maltsev EI, Vlasenko VA, Sobolevskii OA, Sadakov AV, Massalimov BI, Pervakov KS (2020) Upper critical field of a two-band $\text{SrFe}_{2-x}\text{Ni}_x\text{As}_2$ superconductor. *JETP Lett* 111:7. <https://doi.org/10.1134/S0021364020070061>
17. Werthamer NR, Helfand E, Hohenberg PC (1966) Temperature and purity dependence of the superconducting critical field, H_{c2} . III. Electron spin and spin-orbit effects. *Phys Rev* 147:295. <https://doi.org/10.1103/PhysRev.147.295>
18. Hu R, Mun ED, Altarawneh MM, Mielke CH, Zapf VS, Bud'ko SL, Canfield PC (2012) Upper critical fields and two-band superconductivity in $\text{Sr}_{1-x}\text{Eu}_x(\text{Fe}_{0.89}\text{Co}_{0.11})_2\text{As}_2$ ($x = 0.20$ and 0.46). *Phys Rev B* 85:064511. <https://doi.org/10.1103/PhysRevB.85.064511>
19. Wang Z, Xie T, Kampert E, Förster T, Lu X, Zhang R, Gong D, Li S, Herrmannsdörfer T, Wosnitzer J, Luo H (2015) Electron doping dependence of the anisotropic superconductivity in $\text{BaFe}_{2-x}\text{Ni}_x\text{As}_2$. *Phys Rev B* 92:174509. <https://doi.org/10.1103/PhysRevB.92.174509>
20. Gurevich A (2007) Limits of the upper critical field in dirty two-gap superconductors. *Physica C* 456:160–169. <https://doi.org/10.1016/j.physc.2007.01.008>
21. De Gennes P-G (1964) Behavior of dirty superconductors in high magnetic fields. *J Phys Condens Matter* 3:79–90. <https://doi.org/10.1007/BF02422354>
22. Maki K (1966) Effect of Pauli paramagnetism on magnetic properties of high-field superconductors. *Phys Rev* 148:362. <https://doi.org/10.1103/PhysRev.148.362>
23. Gurevich A (2003) Enhancement of the upper critical field by nonmagnetic impurities in dirty two-gap superconductors. *Phys Rev B* 67:184515. <https://doi.org/10.1103/PhysRevB.67.184515>
24. Majumdar A, VanGennep D et al (2020) Interplay of charge density wave and multiband superconductivity in layered quasi-two-dimensional materials: the case of 2H-NbS_2 and 2H-NbSe_2 . *Phys Rev Materials* 4:084005. <https://doi.org/10.1103/PhysRevMaterials.4.084005>
25. Abdel-Hafiez M, Zhao Y, Huang Z et al (2018) High-pressure effects on isotropic superconductivity in the iron-free layered pnictide superconductor BaPd_2As_2 . *Phys Rev B* 97:134508. <https://doi.org/10.1103/PhysRevB.97.134508>
26. Kuzmicheva TE, Muratov AV, Kuzmichev SA, Sadakov AV, Aleshchenko YuA, Vlasenko VA, Martovitsky VP, Pervakov KS, Eltsev YuF, Pudalov VM (2017) On the structure of the superconducting order parameter in high-temperature Fe-based superconductors. *Phys-Usp* 60:419. <https://doi.org/10.3367/UFNe.2016.10.038002>

Publisher's note Springer Nature remains neutral with regard to jurisdictional claims in published maps and institutional affiliations.